Band Structures for 2D Photonic Crystals in Presence of Nonlinear Kerr Effect Calculated by Use of Nonlinear Finite Difference Time Domain (NFDTD) Method

A. Khodabakhsh*, M. K. Moravvej-Farshi* and M. Ebnali-Heidari**

Abstract: In this paper, we report the simulation results for impact of nonlinear Kerr effect on band structures of a two dimensional photonic crystal (2D-PhC) with no defect, a PhC based W1-waveguide (W1W), and also Coupled-Cavity Waveguides (CCWs). All PhC structures are assumed to a square lattice of constant a made of GaAs rods of radius r=0.2a, in an air background. The numerical simulation was performed using the nonlinear finite difference time domain (NFDTD) technique. In doing so, we have normalized the electric field and the electric flux density vectors, and used a multi probe procedure. These have resulted in very accurate dispersion relations that, in turn, have enabled us to make some novel observations. For instance, simulations show that with an increase in the input light intensity (in the nonlinear regime) the band edges for all three PhC structures experience some red shifts. The red shifts observed for CCWs are, of course, larger than the red shifts experienced by other two structures. Furthermore, the numerical results for CCWs also show that the larger the light input intensity, the smaller the corresponding maximum light group velocity becomes. To the best of our knowledge, this is the first instance that such observations on the impact of the nonlinear Kerr effect on the band diagram of 2D-PhC waveguides are reported.

Keywords: Photonic crystal (PhC), Nonlinear Kerr effect, Photonic Band Structures, Dispersion Curve, Waveguides.

1 Introduction

Manipulating nonlinear optical materials for enabling all-optical control of light propagation in optical devices has been of particular interest in recent years [1,2]. This can lead to all-optical logic gates, all-optical signal processing, and all-optical photonic chips. Among the well known platforms for designing these all-optical devises, photonic crystal (PhC) platform offers additional capabilities [3-7]. In PhC platform the light dispersion characteristic can easily be controlled. Such a control can be beneficial in reducing the speed of light significantly that is required in producing so-called slow light [7].

Iranian Journal of Electrical & Electronic Engineering, 2011.
Paper first received 4 Dec. 2010 and in revised form 12 Feb. 2011.
* The Authors are with the School of Electrical and Computer Engineering, Advanced Device Simulation Lab (ADSL), Tarbiat Modares University, P. O. Box 14115-143, Tehran 1411713116, Iran.
Emails: khodabaksh@Novinpardazesh.ir, farshi_k@modares.ac.ir.
** The Author is with the Department of Engineering, University of Shahrekord, Shahrekord, Iran.
Email: ebnali-m@eng.sku.ac.ir.

On the other hand, the major researches on optical devices focus on Si and GaAs due to their developed fabrication processes, integration capabilities, and nonlinear properties. Crystal inversion symmetry, in Si and GaAs, causes the second order nonlinear effects to vanish. However, the third order effect such as Kerr effect becomes important in these materials. Such a nonlinear effect that depends on the intensity of the incident light, can be used to make novel optical devices [5-7, 10-12].

Utilizing suitable designed PhC structures such as Coupled-Cavities Waveguide (CCW), has made it possible to achieve a greatly reduced group velocity. This, in turn, has significantly improved the nonlinear effects due to the slow light enhancement [7].

All these make numerical simulation of nonlinear PhCs crucial for designing new all-optical devices based on either Si or GaAs. Simplicity of implementation and the ability of considering nonlinearities, anisotropy, and even material dispersion are some advantages that make finite-difference time-domain (FDTD) method [8] one of the most suitable numerical tools for this task. However, the main drawback of this method is the

memory criteria and simulation time, which completely depends upon size of computational domain [8-10].

Recently, some research groups have used the plane wave expansion (PWE) [13-15] and the FDTD [16] methods for extracting the band structures of the slow light PhC waveguides. Meanwhile, others have utilized the nonlinear finite difference time domain (NFDTD) technique to study the impact of the Kerr effect on the PhC-waveguides band diagrams [17], behavior of some all optical devices [18,19], third harmonic generation [20], and hysteresis phenomenon [21]. However, none of them have considered the impact of the nonlinear Kerr effect on the band diagram of the PhC structures, except [17] which results are not accurate enough to obtain the group velocity curves in detail. In this paper, we have used the NFDTD method to demonstrate how strong the Kerr effect affects the band structures of various 2D PhC waveguides in the slow light regime. In order to solve the required differential equation for calculating the band structures in presence of the nonlinear Kerr effect, we have employed the periodic boundary condition (PBC) [22] and the Perfect Match Layer (PML) [23] techniques. In our calculations, we have also used the unit cell or super cell approach, as required.

The rest of this paper is organized as follows: Section 2 is dedicated to the numerical method, in which the Yee's standard FDTD algorithm [24] is modified to consider nonlinear Kerr effect. In Section 3, we present the simulation results on various PhC structures with a detailed discussion for each case. Finally this paper is closed by a conclusion in Section 4.

2 Numerical Model

Introducing $\sqrt{\varepsilon_0/\mu_0}$ as a normalizing factor for obtaining the normalized quantities for electric field, **E**, magnetic field, **H**, and electric flux density, **D,** as in [8],

$$\tilde{\mathbf{E}} = \sqrt{\frac{\varepsilon_0}{\mu_0}} \cdot \mathbf{E} \tag{1}$$

$$\tilde{\mathbf{H}} = \mathbf{H} \tag{2}$$

$$\tilde{\mathbf{D}} = \sqrt{\frac{1}{\varepsilon_0 \mu_0}} \mathbf{D} \tag{3}$$

where μ_0 and ε_0 are the free space permeability and permittivity. Notice that the normalization factor of magnetic field is unity. For a Kerr-like nonlinear material with inversion symmetry at molecular level, such as Si, GaAs, KD*P, and liquid crystals, in which the second order susceptibility vanishes, relation between the normalized electric field and flux density is reduced to [1]

$$\tilde{\mathbf{D}} = \left(\varepsilon_r + \tilde{\chi}^{(3)} \left| \tilde{\mathbf{E}} \right|^2 \right) \tilde{\mathbf{E}} \tag{4}$$

in which ε_r is the intensity independent relative dielectric constant of the nonlinear media, and $\tilde{\chi}^{(3)}$ is normalized third order susceptibility given by [1]

$$\tilde{\chi}^{(3)} = \frac{\mu_0}{\varepsilon_0} \chi^{(3)} \equiv \frac{4}{3} \varepsilon_r \mu_0 c n_2 \tag{5}$$

where n_2 is the nonlinear refractive index, in m^2/W. Such normalization helps to minimize the numerical errors when solving the Maxwell's equations by FDTD method. Restricting our analysis to a two dimensional situation (i.e. *x-y* plane), Maxwell's equations in such a nonmagnetic medium can either be written as,

$$\frac{\partial \tilde{D}_z}{\partial t} = \frac{1}{\sqrt{\varepsilon_0 \mu_0}} \left(\frac{\partial H_y}{\partial x} - \frac{\partial H_x}{\partial y} \right) \tag{6}$$

$$\frac{\partial H_x}{\partial t} = -\frac{1}{\sqrt{\varepsilon_0 \mu_0}} \frac{\partial \tilde{E}_z}{\partial y} \tag{7}$$

$$\frac{\partial H_y}{\partial t} = \frac{1}{\sqrt{\varepsilon_0 \mu_0}} \frac{\partial \tilde{E}_z}{\partial x} \tag{8}$$

$$\tilde{D}_z = \left(\varepsilon_r + \tilde{\chi}^{(3)} \left| \tilde{E}_z \right|^2 \right) \tilde{E}_z, \tag{9}$$

for TM mode (E-polarized) for which $E_x = E_y = H_z = 0$,

$$\frac{\partial \tilde{D}_x}{\partial t} = \frac{1}{\sqrt{\varepsilon_0 \mu_0}} \frac{\partial H_z}{\partial y} \tag{10}$$

$$\frac{\partial \tilde{D}_y}{\partial t} = -\frac{1}{\sqrt{\varepsilon_0 \mu_0}} \frac{\partial H_z}{\partial x} \tag{11}$$

$$\frac{\partial H_z}{\partial t} = -\frac{1}{\sqrt{\varepsilon_0 \mu_0}} \left(\frac{\partial \tilde{E}_y}{\partial x} - \frac{\partial \tilde{E}_x}{\partial y} \right) \tag{12}$$

$$\tilde{D}_x = \left[\varepsilon_r + \tilde{\chi}^{(3)} \left(\left| \tilde{E}_x \right|^2 + \left| \tilde{E}_y \right|^2 \right) \right] \tilde{E}_x \tag{13a}$$

$$\tilde{D}_y = \left[\varepsilon_r + \tilde{\chi}^{(3)} \left(\left| \tilde{E}_x \right|^2 + \left| \tilde{E}_y \right|^2 \right) \right] \tilde{E}_y, \tag{13b}$$

for TE mode (H-polarized) for which $H_x = H_y = E_z = 0$.

To solve Eqs. (6)-(9) or (10)-(13) by FDTD numerical method, one should discretize them in both time and space. Such discretization can easily be performed under Yee's cell algorithm [24]. However, in this case we consider the electric flux density equation instead of the one for electric field. For example, assuming the TM mode, one can write

$$\tilde{D}_z^n(i,j) = \left[\varepsilon_r(i,j) + \tilde{\chi}^{(3)}(i,j) \left| \tilde{E}_z^n(i,j) \right|^2 \right] \tilde{E}_z^n(i,j) \tag{14}$$

$$H_x^{n+\frac{1}{2}}\left(i, j+\frac{1}{2}\right) = H_x^{n-\frac{1}{2}}\left(i, j+\frac{1}{2}\right) - \frac{\Delta t}{\sqrt{\varepsilon_0 \mu_0}} \left[\frac{\tilde{E}_z^n(i,j+1) - \tilde{E}_z^n(i,j)}{\Delta y} \right] \tag{15}$$

$$H_y^{n+\frac{1}{2}}\left(i+\frac{1}{2},j\right)=H_y^{n-\frac{1}{2}}\left(i+\frac{1}{2},j\right)+\frac{\Delta t}{\sqrt{\varepsilon_0\mu_0}}\left[\frac{\tilde{E}_z^n(i+1,j)-\tilde{E}_z^n(i,j)}{\Delta x}\right] \quad (16)$$

$$\tilde{D}_z^{n+1}(i,j)=\tilde{D}_z^n(i,j)+\frac{\Delta t}{\sqrt{\varepsilon_0\mu_0}}\times\left\{\left(H_y^{n+\frac{1}{2}}(i+1/2,j)-H_y^{n+\frac{1}{2}}(i-1/2,j)\right)\Big/\Delta x-\left(H_x^{n+\frac{1}{2}}(i,j+1/2)-H_x^{n+\frac{1}{2}}(i,j-1/2)\right)\Big/\Delta y\right\} \quad (17)$$

where superscript n represents the time index, Δt is the time step, Δx and Δy are the grid spacing, and finally i and j represent the grid coordinates in x and y directions, respectively. The discretized equations for TE mode can be obtained in the same manner. As demonstrated by [10], solving the constitutive relation implicitly is the main new step in the NFDTD method added to the conventional Yee's algorithm, which can be implemented by a numerical iterative method like Newton-Raphson method in general form, or an inversing function. The standard Yee's FDTD algorithm is stable under the Courant's stability condition [25], stated that the numerical propagation velocity must be greater than the maximum phase velocity of the electromagnetic waves in the structure, v_{pmax}. For a 2D structure, this condition can be written as

$$\frac{1}{\Delta t\sqrt{(\Delta x)^{-2}+(\Delta y)^{-2}}}\geq v_{pmax} \quad (18)$$

Details of the stability condition for NFDTD algorithm for nonlinear materials are discussed in [10]. It is shown that for any nonlinear material with $\chi^{(3)}>0$ (i.e., for any positive Kerr materials), Courant's stability condition is still sufficient for code stability, due to the decreased local phase velocity of light in these materials. Since the maximum phase velocity, v_{pmax}, in the media under investigation, is always smaller than the velocity of light in the free space, c, so we can rewrite (18) as

$$\frac{1}{\Delta t\sqrt{(\Delta x)^{-2}+(\Delta y)^{-2}}}\geq c\geq v_{pmax}. \quad (19)$$

Now, by assuming an equal grid spacing of

$$\Delta x=\Delta y=2c\Delta t\equiv\frac{2\Delta t}{\sqrt{\varepsilon_0\mu_0}} \quad (20)$$

which satisfies the stability condition of (19), Eqs. (14) to (17) can be simplified,

$$\tilde{D}_z^n(i,j)=\left[\varepsilon_r(i,j)+\tilde{\chi}^{(3)}(i,j)\left|\tilde{E}_z^n(i,j)\right|^2\right]\tilde{E}_z^n(i,j) \quad (21)$$

$$H_x^{n+\frac{1}{2}}\left(i,j+\frac{1}{2}\right)=H_x^{n-\frac{1}{2}}\left(i,j+\frac{1}{2}\right)-\frac{1}{2}\left[\tilde{E}_z^n(i,j+1)-\tilde{E}_z^n(i,j)\right] \quad (22)$$

$$H_y^{n+\frac{1}{2}}\left(i+\frac{1}{2},j\right)=H_y^{n-\frac{1}{2}}\left(i+\frac{1}{2},j\right)+\frac{1}{2}\left[\tilde{E}_z^n(i+1,j)-\tilde{E}_z^n(i,j)\right] \quad (23)$$

$$\tilde{D}_z^{n+1}(i,j)=\tilde{D}_z^n(i,j)+\frac{1}{2}\times\left\{\left[H_y^{n+\frac{1}{2}}\left(i+\frac{1}{2},j\right)-H_y^{n+\frac{1}{2}}\left(i-\frac{1}{2},j\right)\right]-\left[H_x^{n+\frac{1}{2}}\left(i,j+\frac{1}{2}\right)-H_x^{n+\frac{1}{2}}\left(i,j-\frac{1}{2}\right)\right]\right\} \quad (24)$$

The corresponding equations for TE mode can be also simplified by a similar manner.

Relation between the optical signal intensity, I(ω), of radian frequency ω and the normalized electric field intensity is given by

$$I(\omega)=2\sqrt{\varepsilon_r}\varepsilon_0 c\left|E(\omega)\right|^2\equiv 2\sqrt{\varepsilon_r}\left|\tilde{E}(\omega)\right|^2 \quad (25)$$

With the typical values of $\chi^{(3)}$ or Kerr constants for GaAs and Si given in [1] the optical input intensity to be in the nonlinear regime should be in the order of GW-cm^2.

Solving Eqs. (21)-(24) in a suitable computational domain with appropriate boundary conditions, one can obtain the photonic band structure or dispersion relation, numerically. The procedure is the same as what is done in a linear regime, except for the NFDTD equations that are used instead of the linear FDTD's, and also the use of multi probe procedure in the process. Starting with an appropriate **k**-vector in the first Brillouin zone, the NFDTD algorithm is executed over the entire time steps, iteratively over the entire irreducible Brillouin zone. Depending on the chosen k-vector and the computational domain the boundary conditions are taken to be either PBC or PML. In order to obtain the dispersion curves or band diagrams, the electric field components are saved in each time step, for several minimum symmetry points, and then converted into the frequency domain by means of a Fast Fourier Transform (FFT). In order to obtain achieve high accuracy and avoid possible omission eigenvalues, we have post processed all frequency responses, by implementing a multi-probe procedure. This has enabled us obtain more complete and accurate dispersion curves in comparison to those obtained by [17] and hence enables us to achieve accurate group velocity curves in nonlinear regime, especially for CCWs.

Table 1 Geometrical and physical parameters of the PhC structures used in the simulation.

Parameter	Description	Value	Unit
a	Lattice constant	350	nm
r	Rods diameter	70	nm
n_0	linear refractive index (GaAs)	3.4	–
n_2	Kerr coefficient (GaAs)	3.3×10^{-13}	cm^2-W^{-1}

3 Results and Discussion

In this simulation, the PhCs are assumed to be two dimensional (2D) with a square lattice of constant *a* made of GaAs rods of radius r=0.2a in air background. The physical and geometrical parameters of the PhC structures used in this simulation are tabulated in Table 1.

Figure 1 illustrates a schematically cross-sectional view of the PhC lattice and the corresponding first Brillouin zone. The shaded region in Fig. 1(a) illustrates the lattice unit cell that represents the computational domain whose borders are terminated by PBC. The shaded region in Fig. 1(b) illustrates the corresponding irreducible Brillouin zone. The structures under studies are: a conventional PhC without any defect, a PhC-W1-waveguide (PhC-W1W), and three different PhC coupled-cavity waveguides (PhC-CCWs). The light mode propagating in all three waveguides are assumed to be *E*-polarized (TM). Light input intensities in the range of 0.5 GW-$cm^{-2}\leq I\leq$ 25 GW-cm^{-2} were used for all five structures.

3.1 Conventional PhC

First, in order to examine the impact of Kerr effect on the band structure a conventional PhC waveguide, we employ three different input light intensities in the nonlinear regime, given in Table 1.

Figure 2 illustrates and compares the resulting band structures. To our expectation, as seen in Fig. 2, an increase in the input light intensity causes a red shift in the band edge. In fact, at higher intensities the waveguide effective index is more enhanced. This, in turn, reduces the waveguide cut-off wavelength. As a result the larger the increase in intensity the more enhanced is the red shift. Furthermore, this figure shows that in the region where the bands are flatter the red shift is also enhanced. In fact, the flatter the band structure, the slower is the light group velocity ($v_g = \partial\omega/\partial k$) in that region. On the other hand, the slower light has more time to interact with the nonlinear material along the path it propagates. Hence, the slower the light, the more chance it has to enhance the Kerr effect and hence increases the red shift. In comparison to the numerical results obtained by [17], the red shifts in the band structures are very similar, but we have obtained more precise and also complete k vector band structure.

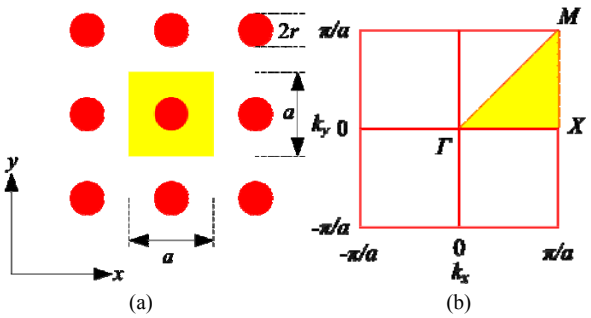

Fig. 1 (a) A schematic cross-sectional view of the 2D PhC structure with a square lattice whose unit cell is shown by the shaded region; (b) The first Brillouin zone of the 2D PhC of Fig. 1(a) whose irreducible Brillouin zone is shown by shaded region.

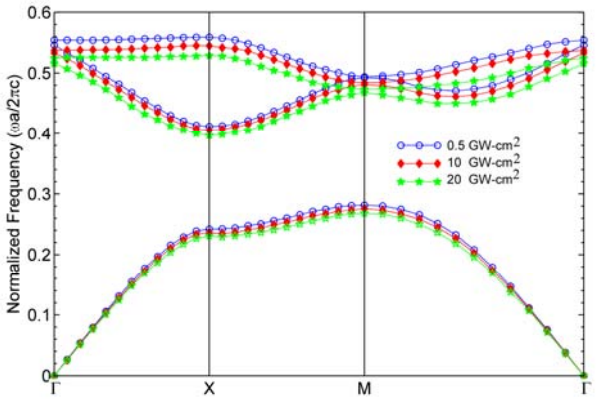

Fig. 2 The three first photonic band structures for the 2D-PhC of Fig. 1, obtained under three different E-polarized illumination with peak input intensities of 0.5GW-cm^{-2} (hollow circles), 10GW-cm^{-2} (diamonds), and 25GW-cm^{-2} (stars) are compared.

3.2 2D-PhC-W1W

In this section, we simulate the band structure of a nonlinear 2D PhC based W1W. This waveguide is made by creating a line defect along the ΓX direction in a conventional 2D PhC-waveguide. A line defect in a pillar based PhC structure is created by removing a row of rods in any direction. A schematic cross sectional view of a 2D PhC-W1W is illustrated in Fig. 3(a). The shaded area, shown in this figure, represents the simulation domain. By utilizing the super cell approach, the boundaries of this domain in *x* and *y* directions are terminated by PBC and PML, respectively.

Figure 3(b) illustrates the simulated band structures of W1W for the three input intensities mentioned earlier. In order to observe the changes in band structure more conveniently, the portion of the band structure surrounded by the dashed rectangle is zoomed out and illustrated in Fig. 3(c). In this illustration, the folded band regions are not shown. The red shift induced by the Kerr effect in the band edges for the higher input

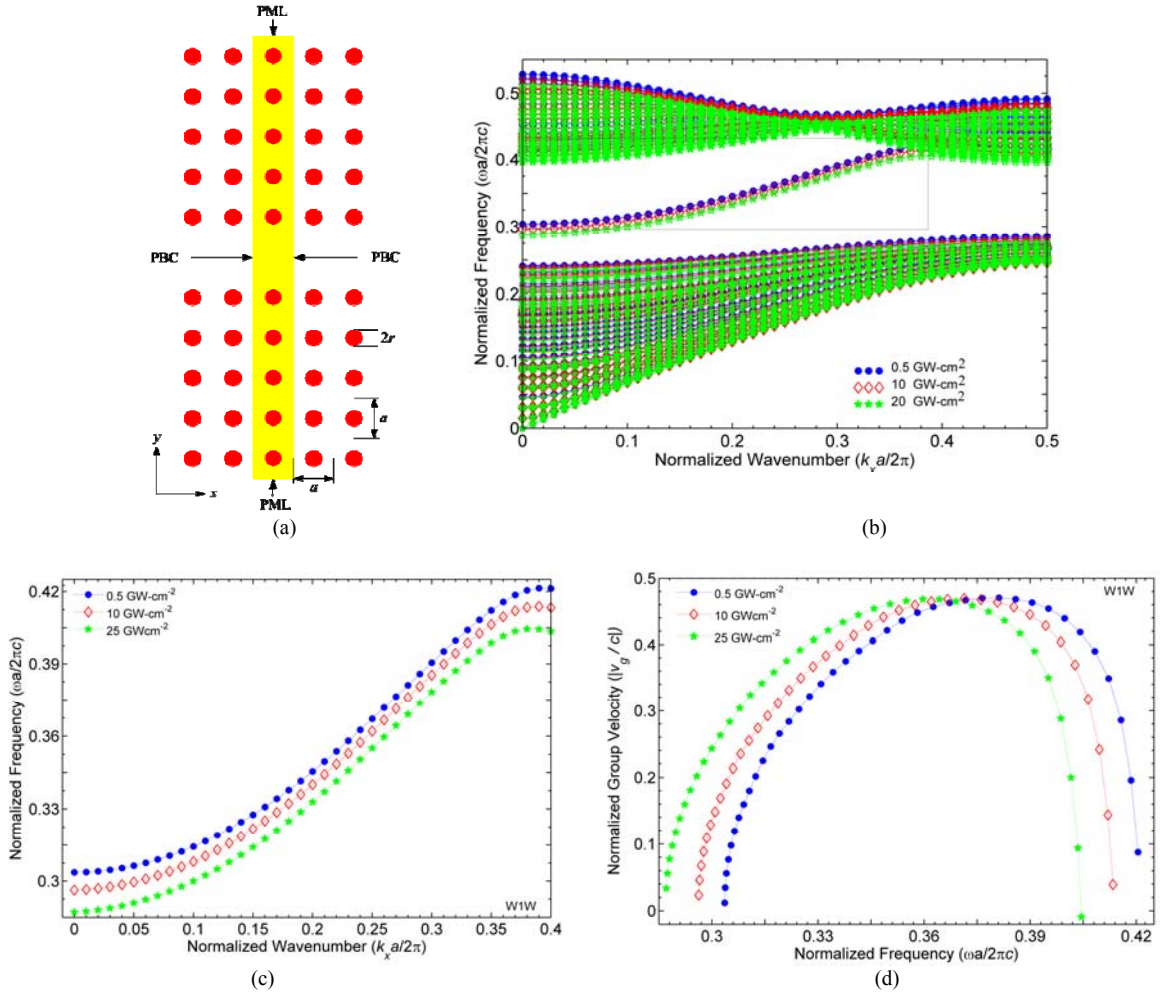

Fig. 3 (a) A schematic cross-sectional view of a 2D-PhC-W1W. The shaded region represents the computational domain (the super cell) whose boundaries are defined PBC and PML in *x* and *y* directions, respectively. (b) The simulated band structures of the waveguide of Fig. 3(a) under three different light intensities. (c) Zoomed out portion of the three dispersion curves, surrounded by the dashed rectangle shown in Fig. 3 (b), while ignoring the folded bands. (d) Normalized group velocities of the three *E*-polarized lights, propagating along W1W of Fig. 3(a), versus the normalized frequency.

intensities can also be observed, similar to the observation made for the conventional PhC waveguide. However, due to the difference in the effective indices of these two waveguide structures, the size of the red shift caused by a given increase in the light intensity is not the same as before. In fact, the red shift observed in Fig. 3(c), in the band edges corresponding to the two higher input intensities, are smaller than those observed in Fig. 2(b) obtained under similar conditions. In fact, by removing a row of GaAs Pillars the Kerr effect has become less effective in the PhC-W1W. Figure 3(d) illustrates the normalized group velocity of the lights propagating in the nonlinear W1W versus the normalized frequency. The flat regions shown in Fig. 3(c) that represent the slow light regions are experiencing the largest red shifts. Also observed in Fig. 3(d), are the maximum group velocities of around v_g~0.47c. As explained before, in this case also, the minimum red shifts in the band edges occur where the group velocities are maximized. The range of the operating bandwidths (normalized and absolute frequencies) for *E*-polarized light modes with intensities in the range of 0.5GW-cm^{-2}≤*I*≤25GW-cm^{-2} propagating along the W1W of Fig. 3(a) is given Table 2. Also given in this table is the average red shift in the band edges corresponding to the minimum and maximum group velocities, induced by an increase of ΔI= 1GW-cm^{-2} in the light intensity. The lattice periodicity is given in Table 1. In comparison to the numerical results obtained by [17], our results demonstrate more red shifts for all normalized k vectors, especially in the flat regions of the dispersion curve. In addition, we have achieved the group velocity curves in nonlinear regime, which are not obtained in [17].

3.3 2D-PhC-CCWs

Exhibition of slow light in 2D-PhC-CCWs has made them a suitable platform for investigating nonlinear effects [5-7]. A 2D-PhC-(CCW) is usually made by creating equally spaced point defects in a row of 2D-PhC, in any direction. A point defect in a pillar based 2D-PhC is created by removal of a rod from the structure. Figure 4 illustrates three different CCW1, CCW2, and CCW3 with cavity spacing of L=2a, 3a, and 4a, respectively. The highlighted region in each case illustrates the super cell (the computational domain) whose boundaries in x and y directions are terminated by PBC and PML, respectively.

In this section, first, we present the dispersion curves simulated for all three CCWs of Fig. 4, obtained under illuminations by the aforementioned three E-polarized lights. Figure 5 illustrates these results, ignoring the folded bands. As can be observed in Fig. 5, in addition to the enhancement of the red shifts in band edges due to the increased input intensities in a particular CCW, an increase in the cavity spacing (L) of a CCW causes the dispersion curves to be flattened over a wider range of wave vectors along the propagation direction. In other words, the larger the cavity spacing L, the slower is the light group velocity propagating throughout the CCW. This is demonstrated in Fig. 6, which illustrates the normalized group velocities of the lights versus the normalized frequency, corresponding to the dispersion curves of Fig. 5. As we have discussed for the other waveguide structures, this means that the light in the CCW with larger L has more time to interact with the waveguide nonlinearity, and hence enhances the red shift. This is due to the fact that the larger the cavity spacing the larger is the effective index of the CCW. In other words, larger L means removal of less nonlinear materials that are replaced by air. Comparison of the corresponding group velocities for the three CCWs illustrated in Fig. 6 also shows this. As observed in this comparison, an increase of ΔL=a in the cavity spacing has resulted in reduction of the maximum group velocities by more than three times, for all three input. In fact, the larger is the cavity spacing the longer it takes for a cavity to amplify the light before it can be coupled to the neighboring cavity. This, in turn, increases the light interaction with the nonlinear material even further. Furthermore, as the light input intensity in a particular CCW structure increases the corresponding maximum group velocity decreases.

Also observed, in Fig. 6, is the effect of the variations in the cavity spacing on the CCWs' operating bandwidths. As the cavity spacing in a given structure increases the corresponding bandwidth for a light mode of a given intensity decreases. Furthermore, as the light mode intensity in a given structure increases the operating bandwidth decrease. The range of the operating bandwidths (normalized and absolute frequencies) for the *E*-polarized light modes with intensities of $0.5\text{GW-cm}^{-2} \le I \le 25\text{GW-cm}^{-2}$ propagating along the three CCWs of Fig. 4, is given in Table 2.

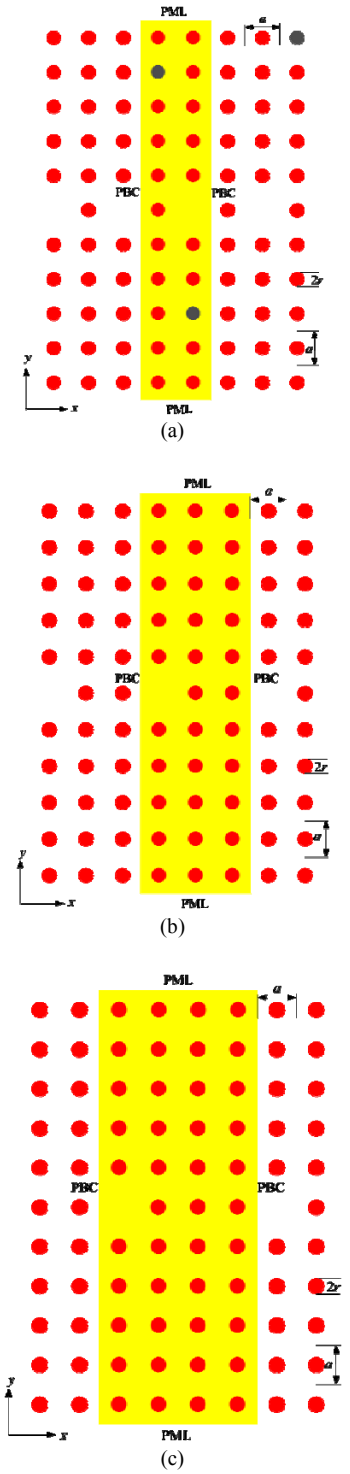

Fig. 4 Schematic representation of cross sectional views of 2D PhC CCW with: (a) L=2a; (b) L=3a; and (c) L=4*a*. The shaded region in each case, illustrates the super lattice (the computational domain) whose boundaries in *x* and y directions are terminated by PBC and PML respectively.

Table 2 The range of the operating bandwidths (normalized and absolute frequencies) for the *E*-polarized light modes of intensities in the range of 0.5GW-cm^{-2}≤*I*≤25GW-cm^{-2} propagating along the W1W of Fig 3(a) and the CCW's of Fig. 4. Also shown are the average red shifts in the band edges corresponding to the minimum and maximum group velocities, induced by an increase of ΔI=1GW-cm^{-2} in the light intensity. The PhCs' lattice parameters are given in Table 1.

PhC	Bandwidth		Average Red Shift per GW-cm^{-2} ($\lvert\Delta f/\Delta I\rvert$)			
			Normalized		MHz	
	Δf_{norm}	Δf (THz)	at v_{gmin}	at v_{gmax}	at v_{gmin}	at v_{gmax}
WW1	0.1083-0.1085	92.83-93	6.7×10^{-4}	8.8×10^{-4}	577.3	752.2
CCW1	0.0332-0.0352	28.46-30.17	5.6×10^{-4}	6.4×10^{-4}	475.8	552.8
CCW2	0.0104-0.0111	8.91-9.51	4.5×10^{-4}	4.8×10^{-4}	384.8	409.3
CCW3	0.0032-0.0036	2.74-3.09	4.7×10^{-4}	4.8×10^{-4}	402.3	409.3

† These values are calculated for I=0.5MW-cm^{-2}.

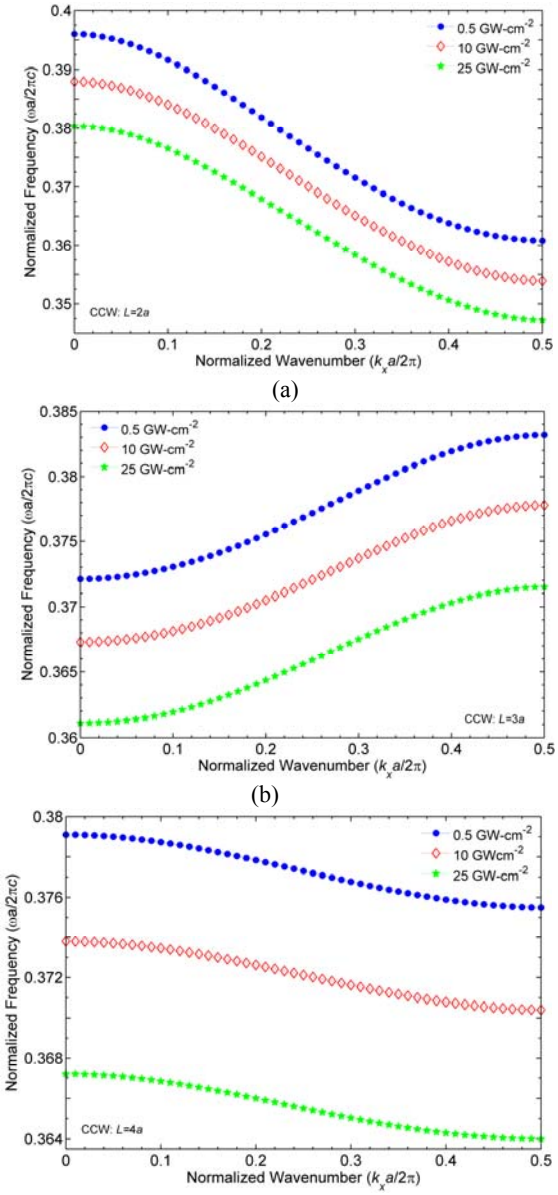

Fig. 5 Illustration of the dispersion curves for the 2D PhC CCWs with cavity spacing of (a) L=2a; (b) L=3a; and (c) L=4a, simulated under illumination by the same *E*-polarized lights used for previous case. For the illustrative purposes, the folded bands are ignored.

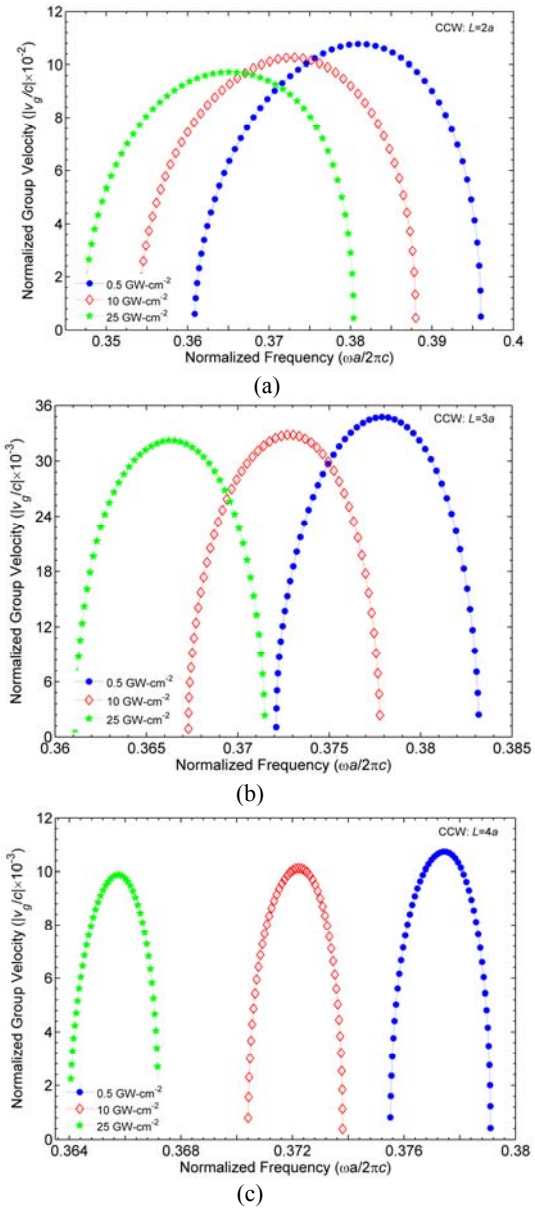

Fig.6 Normalized group velocities of E-polarized lights of various input intensities propagating throughout the CCWs of cavity spacing corresponding to the band structures of Fig. 5 versus the normalized frequency: (a) L=2a, (b) L=3a, and (c) L=4a.

Also given in this table are the average red shifts in the band edges corresponding to the minimum and maximum group velocities, induced by an increase of $\Delta I=1GW\text{-}cm^{-2}$ in the light intensity. The intensity dependence of the operating frequency bandwidth for a particular PhC-CCW structure shows the capability of such waveguides for designing all-optical devices that can be dynamically controlled.

In comparison to the numerical results for CCW2 obtained by [17], our results demonstrate more flat dispersion relations and also more red shifts for all normalized k vectors. In addition, we have achieved the group velocity curves in nonlinear regime. These results demonstrate that the sensitivity of the frequency bandwidth in terms of the light intensity in CCW2 is far more than the results of [17].

4 Conclusion

We have shown that the NFDTD method is capable of simulating the band structure of the nonlinear PhC structures. The band structure of a nonlinear Kerr effect 2D PhC structure is simulated and the dependence of the bands on the input field is observed. The bands and the bandgap are red shifted by the increasing the input field intensity. This red shift can be explained by the intensity dependant refractive index and group velocity of light in the structure, which is relative to the slope of the bands. We have also obtained the dispersion relation of the nonlinear Kerr effect PhC conventional W1 and CCWs, using the NFDTD method. The corresponding red shifts of dispersion curves, which are dependent on the input field intensity, have been demonstrated. Simulations show that the red shift is larger where the dispersion curves are flatter. This is due to the reduced group velocity of light and more time for the propagating light to interact with the nonlinear material. Two interesting effects consist of the reduction in the group velocity of light, and the severe variation in the frequency ranges of the propagating light in the CCWs, both by increasing the input field intensity, have been seen in the simulation results. The former has been explained by the intensity dependant refractive index, and the later seems to be useful in designing all-optical dynamically controlled devices.

Utilization of a multi-probe procedure, and post processing of the FFT responses in NFDTD algorithm, has made it possible to obtain highly accurate and complete band diagrams, resulting in accurate group velocity curves, specifically for CCWs.

References

[1] Boyd R. W., *Nonlinear Optics*, 2nd Ed., Academic Press, 2003.

[2] Banerjee P. P., *Nonlinear Optics: Theory, Numerical Modeling and Applications*, Marcel Dekker, 2004.

[3] Joannopoulos J. D., Johnson S. G., Winn J. N. and Meade R. D., *Photonic Crystals: Molding the Flow of Light,* 2nd Ed.*,* Princeton University Press, 2008.

[4] Sakoda K., *Optical Properties of Photonic Crystals*, Springer-Verlag, 2001.

[5] Mingaleev S. F. and Kivshar Y. S., "Nonlinear transmission and light localization in photonic crystal waveguides", *J. Opt. Soc. Am. B, Opt. Phys*., Vol. 19, No. 9, pp. 2241-2249, 2002.

[6] Mingaleev S. F. and Kivshar Y. S., "Nonlinear photonic crystals: Toward all optical technologies", *Opt. & Phot. News*, Vol. 13, No. 7, pp. 49-51, 2002.

[7] Solja˘ci´c M., Johnson S. G., Fan S., Ibanescu M., Ippen E. and Joannopoulos J. D., "Photonic crystal slow light enhancement of nonlinear phase sensitivity", *J. Opt. Soc. Am. B, Opt. Phys*., Vol. 19, No. 9, pp. 2052-2059, 2002.

[8] Sullivan D. M., *Electromagnetic Simulation Using the FDTD Method*, IEEE Press, 2000.

[9] Lee H. H., Chae K. M., Yim S. Y. and Park S. H., "Finite-difference time-domain analysis of self-focusing in a nonlinear Kerr film", *Opt. Express*, Vol. 12, No. 12, pp. 2603-2609, 2004.

[10] Reinke C. M., Jafarpour A., Momeni B., Soltani M., Khorasani S., Adibi A., Xu Y. and Lee R. K., "Nonlinear finite-difference time-domain method for the simulation of anisotropic, $\chi^{(2)}$, and $\chi^{(3)}$ optical effects", *J. Lightw. Technol.,* Vol. 24, No. 1, pp. 624-634, 2006.

[11] Monat C., Corcoran B., Ebnali-Heidari M., Grillet C., Eggleton B. J., White T. P., O'Faolain L. and Krauss T. F., "Slow light enhancement of nonlinear effects in silicon engineered photonic crystal waveguides", *Opt. Express*, Vol. 17, No. 4, pp. 2944-2953, 2009.

[12] Ebnali-Heidari M., Monat C., Grillet C. and Moravvej-Farshi M. K., "A proposal for enhancing four-wave mixing in slow light engineered photonic crystal waveguides and its application to optical regeneration", *Opt. Express*, Vol. 17, No. 20, pp. 18340-18353, 2009.

[13] Kubo S., Mori D. and Baba T., "Low-group-velocity and low-dispersion slow light in photonic crystal waveguides*", Opt. Lett*., Vol. 32, No. 20, pp. 2981-2983, 2007.

[14] Li J., White T. P., O' Faolain L., Gomez-Iglesias A. and Krauss T. F., "Systematic design of flat band slow light in photonic crystal waveguides", *Opt. Express,* Vol. 16, No. 9, pp. 6227-6232, 2008.

[15] Ebnali-Heidari M., Grillet C., Monat C. and Eggleton B. J., "Dispersion engineering of slow light photonic crystal waveguides using microfluidic infiltration", *Opt. Express*, Vol. 17, No. 3, pp. 1628-1635, 2009.

[16] Krauss T. F., "Slow light in photonic crystal waveguides", *J. Phys. D*, Vol. 40, No. 9, pp. 2666-2670, 2007.
[17] Maksymov I. S., Marsal L. F. and Pallares J., "An FDTD analysis of nonlinear photonic crystal waveguides", *Opt. and Quant. Elec.*, Vol. 38, No. 1-3, pp. 149-160, 2006.
[18] Kosmidou E. P. and Tsiboukis T. D., "An FDTD analysis of photonic crystal waveguides comprising third-order nonlinear materials", *Opt. and Quant. Elec.*, Vol. 35, No. 10, pp. 931-946, 2003.
[19] Qin F., Liu Y., Meng Z. and Li Z., "Design of Kerr-effect sensitive microcavity in nonlinear photonic crystal slabs for all-optical switching", *J. App. Phys.*, Vol. 108, No. 5, pp. 053108-053115, 2010.
[20] Bahl M., Panoiu N. C. and Osgood R. M. Jr., "Nonlinear optical effects in a two-dimensional photonic crystal containing one-dimensional Kerr defects", *Phys. Rev. E*, Vol. 67, No. 5, pp. 056604.1-056604.9, 2003.
[21] Bonnefois J. J., Guida G. and Priou A., "Nonlinear response of a 2D photonic crystal made of Kerr effect nonlinear parallel rods of large diameter," *J. Mod. Opts.*, Vol. 56, No. 5, pp. 646-652, 2009.
[22] Chan C. T., Yu Q. L. and Ho K. M., "Order-N spectral method for electromagnetic waves", *Phys. Rev. B*, Vol. 51, No. 23, pp. 16635-16642, 1995.
[23] Berenger J. P., "A perfectly matched layer for the absorption of electromagnetic waves", *J. Comput. Phys.*, Vol. 114, No. 2, pp. 185-200, 1994.
[24] Yee K. S., "Numerical solution of initial boundary value problems involving Maxwell's equations in isotropic media", *IEEE Trans. Antennas Propag.*, Vol. 14, No. 3, pp. 302-307, 1966.
[25] Cangellaris A. C., "Numerical stability and numerical dispersion of a compact 2-D/FDTD method used for the dispersion analysis of waveguides", *IEEE Microw. Guided Wave Lett.*, Vol. 3, No. 1, pp. 3-5, 1993.

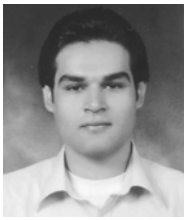

Amir Khodabakhsh was born in Tehran, Iran, on August 28, 1983. He received the B.Sc. degree in electrical engineering from Shahid Beheshty University, Tehran, Iran in 2005 and M.Sc. degree in optical electronics from Tarbiat Modares University, Tehran, Iran in 2008. His research interests are in the fields of photonic crystals, nonlinear optics, slow light, and fiber optic sensors.

Mohammad-Kazem Moravvej-Farshi was born in Yazd, Iran, in 1952. He received the B.Sc. and the M.A. degrees in physics from Sharif University of Technology (SUT), Tehran, Iran, in 1976, and the University of Southern California (USC), Los Angeles, California, in 1978, respectively, the M.Sc. and the Ph.D degrees in electronics from the University of California at Santa Barbara (UCSB), in 1980, and the University of New South Wales (UNSW), Sydney, Australia, in 1987, respectively. From 1980 to 1984, he was a member of research staff with the Division of Microwave, Iran Telecommunication Research Center (ITRC). He joined Tarbiat Modares University (TMU) in 1987, where he is currently a Professor of Electronics. He has translated from English to Farsi four books in the field of semiconductor devices and one in laser electronics. His last translation in 2004 was selected as the best translation of the year in the field of engineering and applied sciences. M. K. Moravvej-Farshi was elected as one of the two most prominent professors of 2002 in the field of electrical engineering, nationwide. He is currently a senior member of IEEE and a senior member of the Optical Society of America (OSA). He is also one of the founders of the Optics and Photonics Society of Iran (OPSI).

Majid Ebnali-Heidari graduated with the BS degree in Electrical Engineering from Isfahan University of Technology, 2003, and the Ms and PhD degrees both in Electrical Engineering from Tarbiat Modares University, in 2005 and 2009 respectively. From 2008 to 2009, he was visiting student at the Centre for Ultrahigh-bandwidth Devices for Optical Systems (CUDOS), School of Physics at the University of Sydney, Australia. Now, he is a faculty member at the Sharekord University, Shahrekord, Iran. His fields of interests are applications of nonlinear optics in photonics, slow light, photonic crystal, and optofluidic devices.